Electron-Transfer-Induced Tautomerization in Methylindanones: Electronic Control of the Tunneling Rate for Enolization

Pawel Bednarek,[†] Z. Zhu,[†,‡] Thomas Bally,*[,†] Tomasz Filipiak,[§] Andrzej Marcinek,[§] and Jerzy Gebicki*[,§]

Contribution from the Institute of Physical Chemistry, University of Fribourg, Perolles, CH-1700 Fribourg, Switzerland, and Institute of Applied Radiation Chemistry, Technical University, 90-924 Lodz, Poland

Received October 17, 2000. Revised Manuscript Received December 27, 2000

Abstract: The radical cations generated from 4-methyl- and 4,7-dimethylindanone, as well as their deuterated isotopomers, isolated in Argon matrices, were found to undergo enolization to the corresponding enol radical cations at rates that differ by orders of magnitude. It is shown by quantum chemical calculations that the effect of the remote methyl group in the 4-position is of purely electronic nature in that it stabilizes the unreactive π-radical relative to the reactive σ-radical state of the 7-methylindanone radical cation. The observed kinetic behavior of the two compounds can be reproduced satisfactorily on the basis of calculated heigth and width of the thermal barrier for enolization, using the Bell model for quantum mechanical tunneling. High-level calculations on the methylacrolein radical cation show that barriers for enolization in radical cations are overestimated by B3LYP/6-31G*.

1. Introduction

Keto−enol tautomerization is a very well understood reaction in organic chemistry.[1] Apart from some notable exceptions,[2] enols are usually less stable[3] and exist only at very low concentration under equilibrium conditions.[4] However, the situation is different in the corresponding radical cations where gas-phase experiments have shown that enol radical cations are usually more stable than their keto tautomers.[5] This is due to the fact that enol radical cations profit from allylic resonance stabilization that is not available to ketones. Moreover, in the case of aromatic carbonyl compounds, enolization results in the formation of *o*-quinoid alcohols that are much easier to ionize than their benzenoid precursors (see Scheme 1).

We have shown that certain classes of radical cations, carrying a wide range of H-donor and H-acceptor groups, undergo spontaneous tautomerization when generated in low-temperature matrices.[6,7] In our earlier studies we had focused mainly on whether enolization does occur or not, but we had already noted that some of these reactions must involve quantum mechanical tunneling.[8,9] In our recent work on the occurrence of electron-transfer induced tautomerization in radical cations of NADH analogues[10,11] we found that the rate of H-transfer depends strongly on the distance and the orientation of the H-donor and the H-acceptor group, and we encountered indeed a borderline case where hydrogen atom tunneling can be observed to occur over hours at 12 K.

Scheme 1

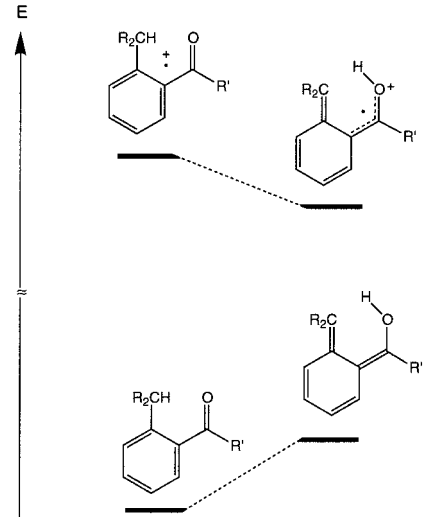

One way to vary the distance over which the hydrogen atom must travel in the course of the enolization is by changing the ring size of the cyclic ketone attached to the tolyl moiety which serves as the H-donor. Since enolization was found to occur spontaneously in 5,8-dimethyltetralone (**DMT**)[9] we thought that

[†] University of Fribourg.

[‡] Present address: Agouron Pharmaceuticals, Alanex Division, San Diego, CA.

[§] Technical University of Lodz.

(1) *The Chemistry of Enols*; Rappoport, Z., Ed.; Wiley: Chichester, 1990.

(2) Hart, H.; Rappoport, Z.; Biali, S. E. Isolable and relatively stable simple enols. In *The Chemistry of Enols*; Rappoport, Z., Ed.; Wiley: Chichester, 1990; p 481.

(3) Guthrie, J. P. Themodynamics of Enols. In *The Chemistry of Enols*; Rappoport, Z., Ed.; Wiley: Chichester, 1990; p 75.

(4) Toullec, J. Keto−Enol Equilibrium Constants. In *The Chemistry of Enols*; Rappoport, Z., Ed.; Wiley: Chichester, 1990; p 323.

(5) Turecek, F. The Chemistry of Ionized Enols in the Gas Phase. In *The Chemistry of Enols*; Rappoport, Z., Ed.; Wiley: Chichester, 1990; p 95.

(6) Gebicki, J. *Pure Appl. Chem.* **1995**, *67*, 55.

(7) Gebicki, J.; Bally, T. *Acc. Chem. Res.* **1997**, *30*, 477.

(8) Gebicki, J.; Marcinek, A.; Michalak, J.; Rogowski, J.; Bally, T.; Tang, W. *J. Mol. Struct.* **1992**, *275*, 249.

(9) Marcinek, A.; Michalak, J.; Rogowski, J.; Tang, W.; Bally, T.; Gebicki, J. *J. Chem. Soc., Perkin Trans. 2* **1992**, 1353.

(10) Marcinek, A.; Adamus, J.; Huzben, K.; Gebicki, J.; Bartczak, T. J.; Bednarek, P.; Bally, T. *J. Am. Chem. Soc.* **2000**, *122*, 437.

(11) Marcinek, A.; Rogowski, J.; Adamus, J.; Gebicki, J.; Bednarek, P.; Bally, T. *J. Phys. Chem. A* **2000**, *104*, 718.

10.1021/ja003708m CCC: $20.00
Published on Web 02/17/2001

by going to the corresponding five-membered ring compound, 4,7-dimethylindanone (**DMI**), we could slow tautomerization sufficiently to monitor the decay of the parent keto radical cation.

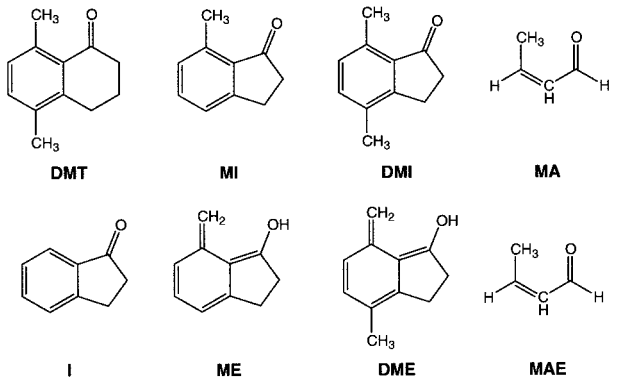

As we will show, this strategy succeeded. However, more importantly, we found that removal of the distant 4-methyl group to give 7-methylindanone (**MI**) has a profound influence on the kinetics of the enolization: $\mathbf{MI}^{\bullet+}$ behaves analogous to $\mathbf{DMT}^{\bullet+}$ rather than $\mathbf{DMI}^{\bullet+}$, in that it decays spontaneously at 12 K in Ar, irrespective of whether it is formed radiolytically from the neutral ketone or by photolysis of the enol radical cation. In the present paper we will put this surprising observation into proper perspective and thus demonstrate for the first time that, next to the more obvious geometric factors, purely *electronic* factors can be instrumental in determining the kinetics of tautomerizations in radical cations. Analogous observations have been made in connection with intra- and intermolecular photoreductions involving *neutral* species many years ago,[12] but to our best knowledge, never in photoenolizations involving compounds of the present type.

2. Experimental Results

Figure 1 shows the spectra obtained after ionization of **DMI** in argon at 12 K (a), after subsequent irradiation at >640 nm (b), and after final irradiation at 490 nm (c). The transformations induced by the two irradiations are represented also in the corresponding difference spectra (b−a and c−b) which show clearly the bleaching and reappearance of a species with sharp absorptions at 600−720 nm. This absorption is typical for the chromophore of the *o*-quinoid radical cations that are formed by tautomerization from radical cations of benzene derivatives substituted vicinally by a H-donor and a H-acceptor group (cf. Scheme 1).[7] In the present case, the expected product is the enol radical cation of **DMI** which we will abbreviate $\mathbf{DME}^{\bullet+}$.

That $\mathbf{DME}^{\bullet+}$ is indeed the product obtained on ionization of **DMI** is also confirmed by the IR spectra in Figure 2, which represent the difference spectra corresponding to (b−a) and (c−b) in Figure 1. They show clearly the decrease of the O−H stretching vibration at 3514 cm^{-1} on >640 nm irradiation, along with other bands in the mid-IR region that match fairly well with those predicted by the results of a B3LYP frequency calculation shown at the bottom of Figure 2. The main IR manifestation of the bleaching of $\mathbf{DME}^{\bullet+}$ is the appearance of a band at 1747 cm^{-1} which corresponds to the C=O stretching vibration of $\mathbf{DMI}^{\bullet+}$, shifted by 27 cm^{-1} to higher energies from that of neutral **DMI**.

(12) See, e.g.: Wagner, P. J. *Acc. Chem. Res.* **1971**, *4*, 168.

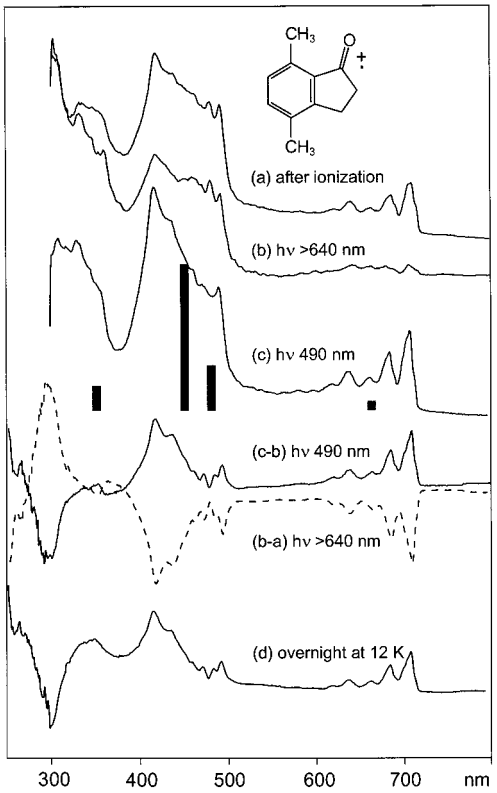

Figure 1. Electronic absorption spectra obtained after ionization of **DMI** in Ar at 1 K (a) and after subsequent irradiation at >640 (b) and 490 nm (c). Difference spectra b−a and c−b highlight the spectral changes during the last two steps. Difference spectrum d was obtained after keeping a sample after >640 nm irradiation during 14 h at 12 K in the dark. Gray bars represent CASPT2 excitation energies and transition moments for $\mathbf{DME}^{\bullet+}$(cf. Table 6).

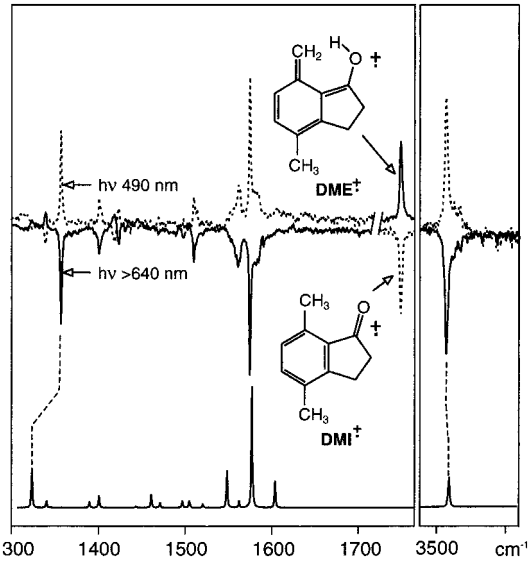

Figure 2. Difference IR spectra for the interconversion of $\mathbf{DMI}^{\bullet+}$ (peaks pointing up in the solid line) and $\mathbf{DME}^{\bullet+}$ (peaks pointing down in the solid line). The bottom spectrum represents the results of a B3LYP/6-31G* frequency calculation on $\mathbf{DME}^{\bullet+}$ (all frequencies scaled by 0.97).

Interestingly, the same transformation that was observed on 490 nm irradiation, i.e., the re-formation of $\mathbf{DME}^{\bullet+}$ from $\mathbf{DMI}^{\bullet+}$, is also witnessed after letting a sample obtained after complete bleaching at >640 nm stand overnight at 12 K (spectrum d in Figure 1). This indicates that enolization of

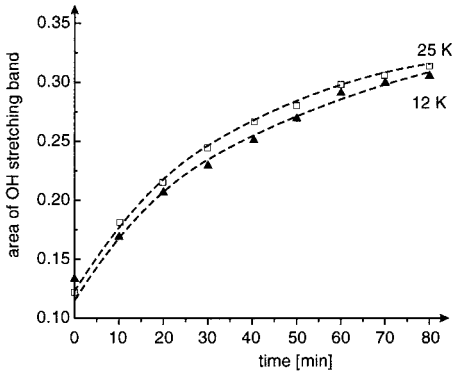

Figure 3. Change in the area of the OH stretching band of **DME**$^{\bullet+}$ with time, starting with a sample of ionizend **DMI** after bleaching **DME**$^{\bullet+}$ by >640 nm irradiation. Similar profiles were obtained at intermediate temperatures and up to 30 K.

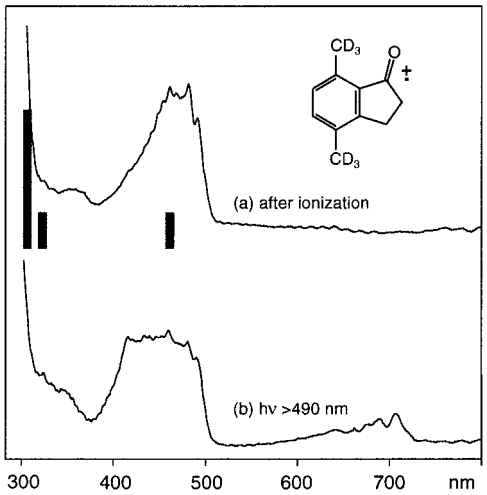

Figure 4. Electronic absorption spectrum obtained after ionization of **DMI-*d*$_3$** in Ar at 12 K (a) and after subsequent irradiation at >590 nm (b). Black bars represent CASPT2 excitation energies and transition moments of **DMI**$^{\bullet+}$ (cf. Table 5).

DME$^{\bullet+}$ occurs also *thermally* at 12 K over hours. Following this reaction by plotting the area under the O−H stretching band in the IR spectrum against time shows that the rate of enolization does not depend on the temperature in the range accessible in Ar matrices (12−30 K) within the error of determination of the band area (the data for 12 and 25 K are shown in Figure 3). This is a strong indication that quantum mechanical tunneling is involved.

This suspicion is confirmed by the experiments with the derivative where the methyl groups are deuterated (**DMI-*d*$_6$**),[13] shown in Figure 4. In contrast to **DMI**, no enolization is observed on ionization, and when the enol is formed photochemically by irradiation at >490 nm (spectrum b in Figure 4), it remains stable over many days at 12 K as well as on warming to 30 K. Thus, the facile enolization that was observed for **DMI**$^{\bullet+}$ is completely suppressed on deutration of the methyl groups. This proves that enolization occurs by tunneling.

Figure 5 shows the results of similar experiments with 7-methylindanone (**MI**) and its deuterated derivative, **MI-*d*$_3$**.[14] As in the case of **DMI**, ionization results in the formation of the corresponding enol radical cation, **ME**$^{\bullet+}$. However, in

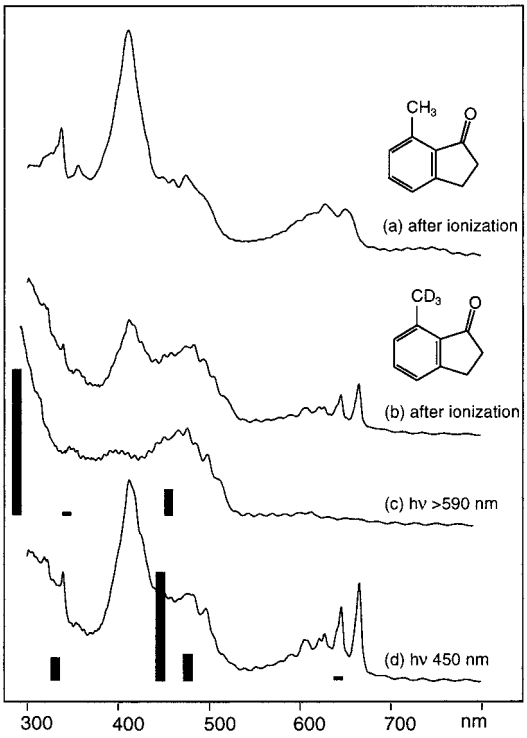

Figure 5. Electronic absorption spectra obtained after ionization of **MI** (a) and **MI-*d*$_3$**, respectively, (b) in Ar at 12 K. (c and d) The spectra after bleaching of **ME-*d*$_3$**$^{\bullet+}$ at >590 nm and its re-formation at 450 nm, respectively. Black bars represent CASPT2 excitation energies and transition moments of **MI**$^{\bullet+}$ (c) and **ME**$^{\bullet+}$ (d).

contrast to the dimethyl derivative, **ME**$^{\bullet+}$ resisted all attempts to convert it back to the parent keto cation, **MI**$^{\bullet+}$, in that the enol cation proved to be entirely photostable at all wavelengths above 350 nm (on prolonged irradiation in the UV some decomposition occurs). That this is not due to an inherent change in the photochemistry on going from **DME**$^{\bullet+}$ to **ME**$^{\bullet+}$ is shown by the results obtained with **MI-*d*$_3$**. Although ionization of this compound results also in partial enolization (spectrum b), this can be reverted photochemically (spectrum c), and the resulting keto cation, **MI-*d*$_3$**$^{\bullet+}$, is entirely stable, unless it is exposed to 450 nm irradiation, whereupon it reverts back to the enol radical cation, **ME-*d*$_3$**$^{\bullet+}$ (spectrum d). The above findings are confirmed by IR spectra corresponding to those shown in Figure 2.

An intriguing aspect of the spectra shown in Figure 5 is the difference in shape and the shift between the first absorption bands of **ME**$^{\bullet+}$ and its deuterated derivative (the shift in the first peak is 325 cm^{-1}!). We have no explanation for this phenomenon which was, however, observed in different series of experiments with compounds whose identity had been scrupulously ascertained.

Thus, the experiments described above show unambiguously that the presence or absence of a methyl group in what appears to be a pure "spectator" position has a profound influence on the rate of enolization in the radical cation of 4-methylindanone. Its presence slows the reaction from less than minutes at 12 K (i.e. the time it takes to observe the spectrum of the enol radical cation after bleaching) to several hours at 12−30 K. As we will show, the explanation of this surprising phenomenon resides in the photoelectron spectra of the two compounds (Figure 6)

(13) For reasons of economy, *per*deuterio *p*-xylene was employed in the synthesis. Thus, the two remaining aromatic positions in **DMI** are also deuterated, but this is not expected to affect the spectroscopic or kinetic data.

(14) In actual fact, the compound contains an additional deuterium atom in the CH_2 group adjacent to the benzene ring (see Synthesis section). However, this deuterium atom does not affect the spectroscopic or kinetic features of interest in the present study. Therefore, and to avoid confusion, we will designate this compound **MI-*d*$_3$** anyway.

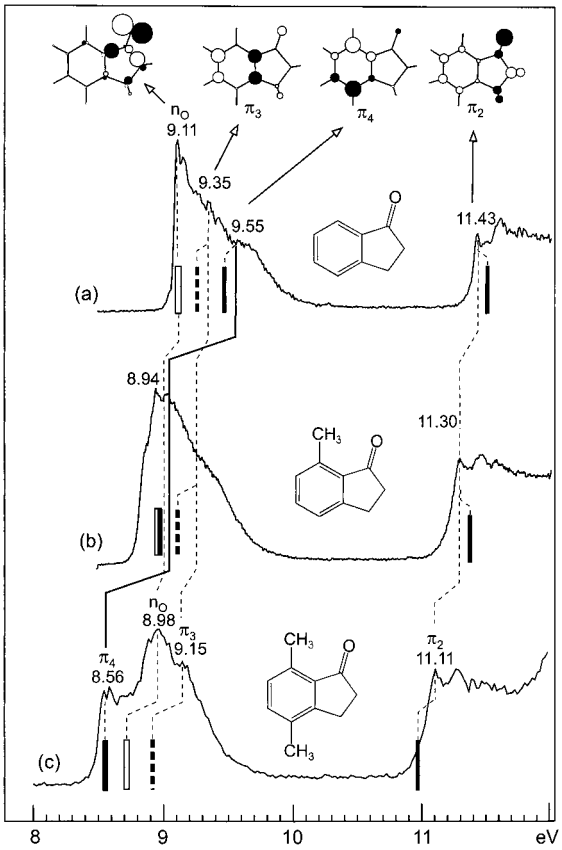

Figure 6. Photoelectron spectra of indanone (a), **MI** (b), and **DMI** (c). The bars are schematic representations of the CASPT2 results listed in Table 1. MOs at the top are from HF-3-21G calculations on neutral indanone.

which will be discussed in the following section, based on quantum chemical calculations.

3. Calculations and Discussion

3.1. The Photoelectron Spectra of Indanones. To our best knowledge the photoelectron (PE) spectra of indanones have not been published to date, and since these spectra form a very good starting point for the ensuing discussion we will begin by their assignment. The PE spectra of related carbonyl-substituted benzenes, such as benzaldehyde or acetophenone, have been published in the 1970s.[15−17] Unfortunately these spectra do not lend themselves to assignment on the basis of Koopmans' theorem, because the orbital energy of the n lone pair (n_O) is invariably predicted much too low relative to those of the π MOs by ab initio Hartree−Fock calculations. Although this can be rectified by resorting to semiempirical methods, different such procedures gave a different ordering of states in benzaldehyde[15] such that no unambiguous assignments of the PE spectra of Ph-COR derivatives have been provided to date. Thus we decided to address this question by the CASSCF/CASPT2 method which has recently proven to be quite reliable in assigning electronic spectra of the Ph-COR type radical cations.[18] In addition we will estimate the important difference between their lowest energy π- and σ-radical states by the B3LYP density functional method. Note that we will not use either method to predict *absolute* ionization energies, but only the energies of excited states *relative to the ground states* of radical cations, as given in Table 1. Below we will use designations $(\mu)^{-1}$ to denote radical ion states attained be electron ejection from MOs ψ_μ of the neutral precursor.

Table 1. Relative Energies (in kcal/mol corrected for zero-point vibrational energy (ZPVE) differences at equilibrium geometries relative to the most stable state) for Different States of $\mathbf{I}^{\bullet+}$, $\mathbf{MI}^{\bullet+}$, and $\mathbf{DMI}^{\bullet+}$ at Different Geometries. Energies

	method →	B3LYP/6-31G*		CASPT2/ANO[a]		
	geometry[b] ↓	$1^2A''$	$1^2A'$	$1^2A''$	$1^2A'$	$2^2A''$
$\mathbf{I}^{\bullet+}$	neutral	9.0	(0)	3.5	(0)	
$\mathbf{DMI}^{\bullet+}$	neutral	4.3	8.1	5.6	11.1	13.6
	$^2A''$ (π-radical)	(0)[c]	14.0	(0)[d]	18.7	18.5
	$^2A'$ (σ-radical)	9.6	6.6[e]	11.0	11.3	15.9
$\mathbf{MI}^{\bullet+}$	neutral	4.2	2.8	1.3	1.1	6.7
	$^2A''$ (π-radical)	(0)[f]	8.7	(0)[g]	9.7	15.3
	$^2A'$ (σ-radical)	9.3	1.4[h]	9.0	5.4	10.3

[a] For active spaces, see footnotes to Tables 4 and 5. [b] Optimized at the B3LYP/6-31G* level. [c] Total energy: −501.345984 hartrees; ZPVE=124.1 kcal/mol. [d] Total energy: −499.738527 hartrees. [e] ZPVE = 124.5 kcal/mol. [f] Total energy: −462.0163499 hartrees; ZPVE = 107.5 kcal/mol. [g] Total energy: −460.585542 hartrees. [h] ZPVE =112.2 kcal/mol.

Indanone: All our calculations agree in predicting that the ground state of the indanone radical cation, $\mathbf{I}^{\bullet+}$, at the geometry of neutral **I** (indicated by an open bar in Figure 6) arises by ionzation from the n_O orbital that extends into the C−C σ-bonds adjacent to the carbonyl group. The first excited state of the radical cation corresponds to ionization from the "bis-ethylenic" π MO of the benzene moiety, $(\pi_3)^{-1}$ (dashed bar in Figure 6), whereas the next one is formed by electron loss from the "bis-allylic" benzene MO, $(\pi_4)^{-1}$ (filled bar).[19] Following a "hole" in the PE spectrum, the next band is due to ejection of an electron from the $\pi_{C=O}$ MO (combined to some extent with CH_2 pseudo-π MOs and the totally symmetric benzene π MO).

The above sequence of the $(n_O)^{-1}$ and the $(\pi_3)^{-1}$ states of $\mathbf{I}^{\bullet+}$ is confirmed by B3LYP calculations. The two methods differ somewhat in their prediction of the gap between these two states (0.15 eV by CASPT2, 0.39 eV by B3LYP). If we assume that the ordering of states given by the two methods is indeed correct, then the PE spectrum indicates that the gap is actually around 0.25 eV. Thus, CASPT2 seems to underestimate sligthly the energy difference between states attained through ionization from n_O and from π MOs, whereas B3LYP overestimates this difference by a similar amount.

4,7-Dimethylindanone: According to our calculations, the state ordering is changed on attaching two methyl groups in the 4- and 7-positions of indanone. The ground state of $\mathbf{DMI}^{\bullet+}$ corresponds to loss of an electron from the π_4 MO which has thus been destabilized by almost 1 eV from its position in indanone, owing to the inductive effect and hyperconjugation with the CH_3 groups.[20] According to our calculations, the peak at 8.98 eV should be assigned to the $(n_O)^{-1}$ state. Note that it has moved only 0.13 eV from its position in parent $\mathbf{I}^{\bullet+}$, in agreement with the fact that the n_O MO does not extend much into the benzene ring. The splitting between the lowest π- and

(15) Rabalais, J. W.; Colton, R. J. *J. Electron Spectrosc.* **1972**, *1*, 83.
(16) Kobayashi, T.; Nagakura, S. *Bull. Chem. Soc. Jpn.* **1974**, *47*, 2563.
(17) Egdell, R.; Green, J. D.; Rao, C. N. R. *Chem. Phys. Lett.* **1975**, *33*, 300.
(18) Huben, K.; Zhu, Z.; Bally, T.; Gebicki, J. *J. Am. Chem. Soc.* **1997**, *119*, 2825.

(19) The numbering of the π MOs shown in Figure 6 is not in line with their ordering in indanone, but with that in **MI** and **DMI**.
(20) This shift is about 20% larger than that on going from benzene to *p*-xylene [Lias, S. G. In *NIST Chemistry WebBook*; NIST Standard Reference Database No. 69; Mallard, W. G., Linstrom, P. J., Eds.; National Institute of Standards and Technology, Gaithersburg MD, 20899, February 2000 (http://webbook.nist.gov)]. This is probably due to the fact that the π_4 MO is lowered by 0.3 eV relative to its position in benzene and can therefore undergo more hyperconjugative interaction with the CH_3 pseudo-π MOs which leads to a stronger destabilization of the π_4 MO.

σ-radical states (0.42 eV from the PE spectrum) is again underestimated, both by CASPT2 (0.24 eV) and B3LYP (0.16 eV). The next excited state of **DMI**$^{\bullet+}$ is the $(\pi_3)^{-1}$ state, 0.35 eV above the ground state according to CASPT2 (0.59 eV from the PE spectrum).

7-Methylindanone: The PE spectrum of **MI**$^{\bullet+}$ is the most difficult one to assign because the first three ionization events are lumped together in a single, barely structured PE band. However, in view of the above assignments this is not surprising, because a linear interpolation between the ionization energies of **I** and **DMI** leads to predicted values of 9.05 eV for both the $(n_O)^{-1}$ and the $(\pi_4)^{-1}$ states and 9.25 eV for the $(\pi_3)^{-1}$ state of **MI**$^{\bullet+}$, in good accord with the observed PE spectrum. Indeed, theory agrees with the finding that the $(n_O)^{-1}$ and the $(\pi_1)^{-1}$ states are nearly degenerate in **MI**$^{\bullet+}$. Both CASPT2 and B3LYP slightly favor the σ-radical over the π-radical ground state, but in view of the above errors in the predicted gaps between these two states in **I**$^{\bullet+}$ and **DMI**$^{\bullet+}$, this prediction should be taken with a grain of salt.

In conclusion, the PE spectra of the three compounds show that there exist substantial differences in the relative energies of the π- and the σ-radical states of the radical cations. We will demonstrate below that the different reactivity with regard to enolization observed for **MI**$^{\bullet+}$ and **DMI**$^{\bullet+}$can be traced back to differences in these σ/π gaps.

3.2. The Mechanism of Enolization in β-Alkylenones: Model Calculations. Photoenolization in β-alkylenones is thought to occur by abstraction of a H atom from the alkyl group by the singly occupied p_σ NBMO of the carbonyl moiety in its triplet n $\rightarrow \pi^*$ excited state, followed by a twisting of the CH_2 group in the incipient diradical to give the ground-state enol (after intersystem crossing which occurs during this last event).[21] By analogy, one may picture enolization in the corresponding radical cations (where it is exothermic, see Introduction) to follow the same mechanism, with the exception that no change in the spin state is required on the way from reactant to product (cf. Figure 7).

This picture is confirmed by calculations on the simplest such system, 3-methylacrolein (**MA**), whose radical cation has a σ-radical ground state. The reaction profile for enolization of **MA**$^{\bullet+}$ to its enol form, **MAE**$^{\bullet+}$, involves indeed a transition state, **TS1**, where the hydrogen atom is roughly halfway between the donor C- and the acceptor O-atoms ($r_{C\cdots H} = 1.35$ Å, $r_{O\cdots H} = 1.23$ Å), but remains in the plane of the molecule. On the far side of **TS1** the reaction proceeds to another transition state, **TS2**, which turns out to be that for rotation of the CH_2 group in the product, the *Z*-butadien-1-ol radical cation (cf. Figure 8). According to IRC calculations this rotation, and hence the loss of C_s symmetry, only sets in after the H has been almost fully transferred to the O-atom. Thus, enolization proceeds diabatically on the $^2A'$ surface of β-alkylenone radical cations.

To examine the validity of the B3LYP/6-31G* method for calculating the activation parameters of such reactions, we first reoptimized the geometries of the three stationary points with larger basis sets at the B3LYP level, and finally also with the QCISD/6-31G* method. For **MA**$^{\bullet+}$ and **MAE**$^{\bullet+}$ the bond lengths vary by less than 0.01 Å between the different methods so that, with regard to these equilibrium geometries, the B3LYP/6-31G* method appears to be appropriate. For **TS1** some of the differences were found to be more important: at the QCISD level the hydrogen atom is closer to the carbon ($r_{C\cdots H} = 1.26$ Å) than to the oxygen atom ($r_{O\cdots H} = 1.33$ Å),[22] in contrast to B3LYP where the opposite is true (see above; the other bond lengths are again within 0.01 Å for both methods). This difference in the geometry of **TS1** changes $\Delta E_0^{\ddagger}$ by -0.88 kcal/

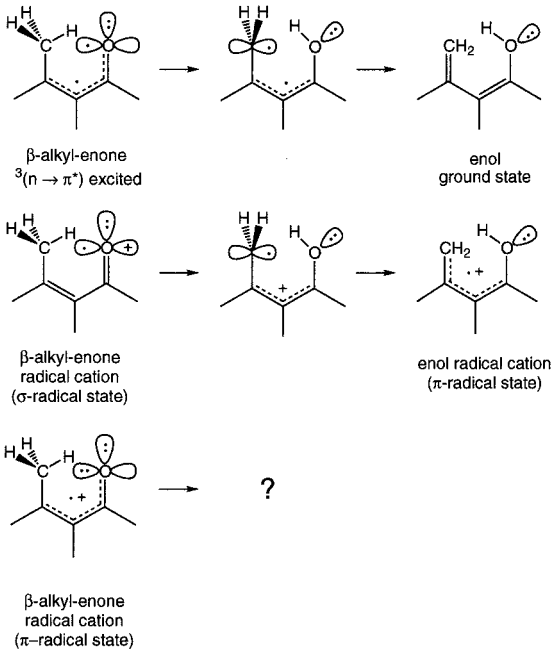

Figure 7. Schematic representation of the mechanism of photoenolization (top) of β-alkylenones and of the corresponding reaction in the corresponding radical cations (bottom). Note that π-radical states of β-alkylenones are unreactive toward enolization.

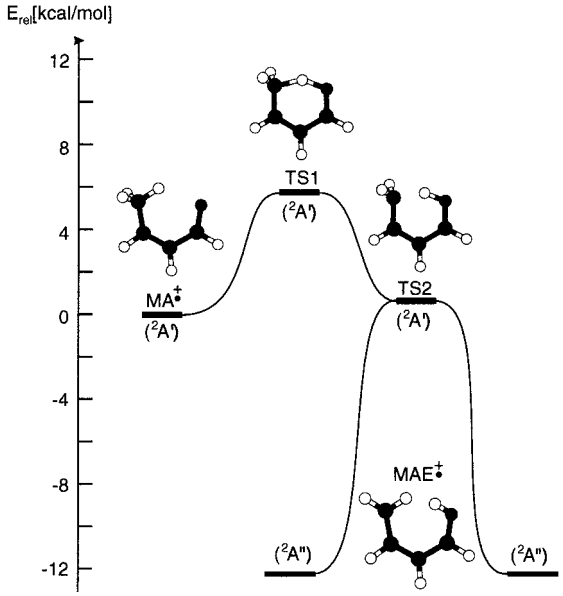

Figure 8. Schematic reaction profile for the enolization of methylacrolein radical cation (**MA**$^{\bullet+}$) as computed by B3LYP/6-31G*. Note that the entire H atom transfer takes place in the $^2A'$ ("σ- radical") state.

(21) See, e.g.: Wagner, P. J.; Chen, C. P. *J. Am. Chem. Soc.* **1976**, *98*, 239.

(22) For reasons of computational economy, we had to impose C_s symmetry in the QCISD optimizations as well as in the B3LYP structures used in the coupled-cluster calculations. In the case of **TS1** this resulted in a stationary point with *two* imaginary normal modes. One of them corresponds to a slight twisting of the CH_2 group, but the associated frequency is only -110 cm^{-1}. Reoptimization in C_1 resulted in a decerase in the B3LYP/6-31G* energy of 0.14 kcal/mol, and in a concomitant increase of the ZPVE of 0.15 kcal/mol. Since the two effects cancel almost exactly, the error in $\Delta E_0^{\ddagger}$ introduced by this approximation should be minimal.

Table 2. 0 K Exothermicities, ΔE_0, and Activation Barriers, $\Delta E_0^{\ddagger}$, for Enolization of $\mathbf{MA}^{\bullet+}$ to $\mathbf{ME}^{\bullet+}$ via **TS1** at Different Levels of Theory

method →	B3LYP[a]				CCSD[b]		CCSD(T)[b]	
basis set ↓	ΔE_0	ΔZPVE	$\Delta E_0^{\ddagger}$	ΔZPVE	ΔE_0	$\Delta E_0^{\ddagger}$	ΔE_0	$\Delta E_0^{\ddagger}$
6-31G*	11.41	2.30	5.85	2.13	12.92	7.73	12.60	5.72
cc-pVDZ	14.26	2.71	3.35	2.21	14.26	4.79	14.19	3.00
6-311G**	15.05	2.78	4.13	2.13	15.09	4.91	15.31	2.73
cc-pVTZ	16.01	2.76	3.70	2.19	17.16	3.61	17.57	1.13

[a] All species fully optimized and corrected for ΔZPVE (as listed in the adjacent columns) with the corresponding basis set. [b] At the B3LYP/6-31G* geometries in C_s symmetry,[22] including ZPVE differences of 2.76 ($\mathbf{MA}^{\bullet+}$/**TS1**) and 2.19 kcal/mol ($\mathbf{MA}^{\bullet+}$/$\mathbf{ME}^{\bullet+}$), respectively, obtained at the same level.

mol at the B3LYP level. We conclude from this that taking B3LYP geometries for the transition states for such tautomerizations introduces an error of ±1 kcal/mol in the calculated $\Delta E_0^{\ddagger}$.

In a second step we carried out single-point calculations by the coupled cluster method, using again different basis sets.[22] The corresponding results, listed in Table 2, indicate that the barrier for enolization of $\mathbf{MA}^{\bullet+}$ appears to be considerably overestimated by B3LYP/6-31G*. Interestingly, this does not become evident when basis sets of DZ-quality are employed, and/or if triple exciations are excluded from the CC treatment. However, at the CCSD(T)/cc-pVTZ level, the classical barrier drops to almost 1 kcal/mol after subtraction of the ZPVE difference between $\mathbf{MA}^{\bullet+}$ and **TS1**.[23] If one employs the QCISD geometries for $\mathbf{MA}^{\bullet+}$ and **TS1**, the barrier increases by 0.9 kcal/mol at the CCSD(T)/cc-pVTZ level, in line with the above estimate of the error introduced by the choice of the B3LYP geometry for **TS1**.

From the above findings we conclude that enolization proceeds diabatically in the σ-radical state of β-alkylenone radical cations to the transition state for CH_2 rotation in the resulting enol radical cations, but that the B3LYP/6-31G* method overestimates barriers for such enolizations by about 5 kcal/mol. The disruption of the aromatic π-system on enolization of methylindanone radical cations from their σ-radical states will lead to some changes in the thermochemistry and, hence, also in the activation parameters for this reaction, but it is not expected that the general mechanism is affected.

More importantly, however, the question arises if and how enolization will proceed if the ground state of an enone is of π-radical nature, in which case the oxygen p_σ NBMO is doubly occupied and hence poorly predisposed to function as an acceptor orbital for the migrating hydrogen atom (see Figure 7). Will the partially vacant p_π-AO of the oxygen atom function as an acceptor, thus necessitating a nonplanar transition state for enolization, or will it be more economical to promote the system to the reactive σ-radical state to effect hydrogen migration? Before looking into this question, we need to assess the nature of the ground states of the methylindanone radical cations *at their equilibrium geometries*.

3.3. Energies of π- and σ-Radical States of Methylindanones. To this end we carried out geometry optimizations of both the π- and the σ-radical states of $\mathbf{MI}^{\bullet+}$ and $\mathbf{DMI}^{\bullet+}$. Since the two states differ by their symmetry with regard to the plane containing the heavy atoms, geometries can be obtained with the economical B3LYP method which has proven above to be quite reliable for providing equilibrium geometries. The results of this exercise are depicted schematically in Figure 9 while the relative energies are listed in Table 1 (absolute energies and geometries of all stationary points are available in the Supporting Information).

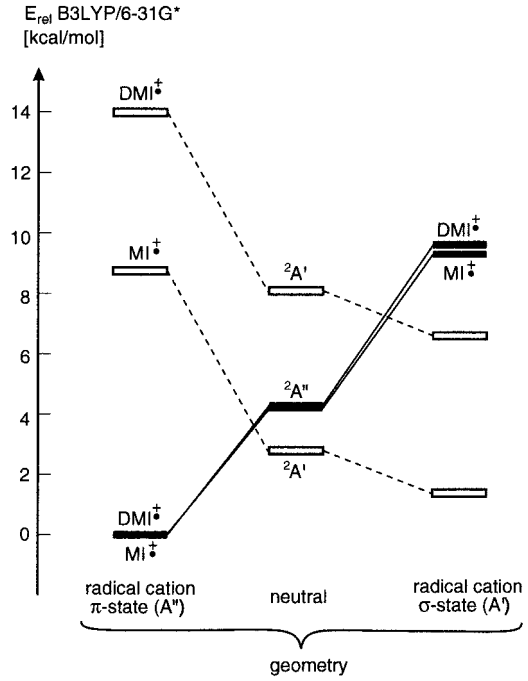

Figure 9. Energy profile for the enolization of $\mathbf{MI}^{\bullet+}$ and $\mathbf{DMI}^{\bullet+}$ according to B3LYP/6-31G* calculations. All energies are relative to the π-radical ground state of the two methylindanone radical cations. For a discussion see the text.

From Figure 9 it becomes apparent that the behavior of $\mathbf{MI}^{\bullet+}$ and $\mathbf{DMI}^{\bullet+}$ on geometry optimization of the $1^2A'$ and the $1^2A''$ states is very similar: in both cases, relaxation of the π- and σ-radical states from the neutral geometry leads to stabilizations of about 4.3 and 1.5 kcal/mol, respectively, while the "opposite" state is destabilized by 5.9 and 5.2 kcal/mol, respectively. This is in line with the observation that the geometries of the two states are very similar in both cases (cf. Supporting Information). Thus, the methyl group in the 4-position has no discernible influence on the changes in structure and energy on relaxation from the neutral geometry.

However, although $\mathbf{MI}^{\bullet+}$ and $\mathbf{DMI}^{\bullet+}$ have different ground states at their neutral geometries (cf. 3.1) the π-radical state is predicted to be more stable after relaxation in both cases, albeit not by much in the case of $\mathbf{MI}^{\bullet+}$. This is in line with the observation of optical spectra for these cations ($\mathbf{DMI}^{\bullet+}$, Figure 4a; $\mathbf{MI}^{\bullet+}$, Figure 5c) which are in good agreement with CASPT2 predictions for species with π-radical ground states, whereas the excited-state structure of the corresponding σ-radical cations would be incompatible with these spectra (see Section 3.4). Thus we conclude that on ionization in Ar the π-radical states of $\mathbf{MI}^{\bullet+}$ and $\mathbf{DMI}^{\bullet+}$ are formed and that enolization must occur from these states.

Thus we proceeded to evaluate the activation parameters for enolization of the two methylindanone radical cations by searching for transition states analogous to **TS1** and **TS2** in Figure 8. The results are listed in Table 3 which shows that, if one takes the energies of the relaxed σ-radical states of $\mathbf{MI}^{\bullet+}$ and $\mathbf{DMI}^{\bullet+}$ as a reference, the 0 K exothermicity ΔE_0 for

(23) Unfortunately we found it impossible to employ higher members of Dunning's series of correlation-consistent basis sets, which would have permitted an extrapolation of the CCSD(T) results to the complete basis set (CBS) limit. However, in view of the almost 2 kcal/mol decrease on going from the double- to the triple-ζ basis set, it is to be expected that the barrier for enolization of $\mathbf{MA}^{\bullet+}$ will disappear almost completely at the CBS limit.

Table 3. Energetics of the Enolization of $\mathbf{MI}^{\bullet+}$, and $\mathbf{DMI}^{\bullet+}$ Evaluated at the B3LYP/6-31G* Level (all energies are relative to the σ-radical state (^{2}A′) at its equilibrium geometry)

	ΔE	ΔZPVE	$\Delta E + \Delta$ZPVE
$\mathbf{DMI}^{\bullet+}$ (^{2}A′)	(0)[a]	(0)[b]	(0)
$\mathbf{DMI}^{\bullet+}$ (^{2}A″)	−6.2	−0.4	−6.6
TS1	+12.3	−2.6	+9.7
TS2	+3.6	±0	+3.6
$\mathbf{DME}^{\bullet+}$	−10.1	1.7	−8.4
$\mathbf{MI}^{\bullet+}$ (^{2}A′)	(0)[c]	(0)[d]	(0)
$\mathbf{MI}^{\bullet+}$ (^{2}A″)	−0.5	−0.9[e]	−1.4
TS1	+11.4	−3.0	+8.4
TS2	+3.6	−0.7	+2.9
$\mathbf{ME}^{\bullet+}$	−8.9	+0.5	−8.4

[a] Total energy = −501.33610 hartrees. [b] ZPVE = 124.1 kcal/mol. [c] Total energy = −462.01571 hartrees. [d] ZPVE = 107.5 kcal/mol (PBE1PBE value: 107.2 kcal/mol). [e] Due to a problem with the vibrational calculation with the B3LYP functional we resorted the PBE1PBE functional for the calculation of the ZPVE (108.1 kcal/mol).

enolization is the same in both cases (−8.4 kcal/mol). In line with qualitative expectations (disruption of the aromatic π-system in the σ-radical state on enolization) ΔE_0 is smaller by about 4 kcal/mol than in $\mathbf{MA}^{\bullet+}$. Consequently, the activation energies $\Delta E_0^{\ddagger}$ are a few kcal/mol higher than in $\mathbf{MA}^{\bullet+}$, but they also differ by only 0.9 kcal/mol (1.3 kcal/mol after ZPVE correction) between $\mathbf{MI}^{\bullet+}$ and $\mathbf{DMI}^{\bullet+}$.

However, if we evaluate the exothermicities and the activation barriers for enolization relative to the π-radical ground states of $\mathbf{MI}^{\bullet+}$ (ΔE_0 = −6.0 kcal/mol, $\Delta E_0^{\ddagger}$ = 9.8 kcal/mol) and $\mathbf{DMI}^{\bullet+}$ (ΔE_0 = −1.8 kcal/mol, $\Delta E_0^{\ddagger}$ = 16.3 kcal/mol) then differences of 4.2 kcal/mol in ΔE_0 and 6.5 kcal/mol in $\Delta E_0^{\ddagger}$ turn up. The latter difference is largely due to the higher energy that is required to promote the keto radical cation to the reactive σ-radical state in the case of $\mathbf{DMI}^{\bullet+}$.[24] Thus, the effect of the methyl group in the 4-position is not on the energetics of the enolization per se as it proceeds from the reactive σ-radical state, but on the energy of the unreactive π-radical ground state which is stabilized by 5.2 kcal/mol in $\mathbf{DMI}^{\bullet+}$ as compared to $\mathbf{MI}^{\bullet+}$. An exhaustive search for alternative transition states that would allow a hydrogen atom transfer directly from the π-radical state did not lead to any stationary points, hence we conclude that enolization must proceed through the σ-radical state.

It is interesting to note that, with ΔE_0 = −1.8 kcal/mol, $\mathbf{DMI}^{\bullet+}$ is a borderline case with regard to spontaneous enolizaton. Attachment of more electron releasing substituents to the benzene ring of indanone or extension of the π-system will stabilize the π-radical state to the point where enolization becomes endothermic. As a matter of fact, the methylfluorenone analogue of **MI** gives a spectrum on ionization in Ar that is very similar to that of parent fluorenone, with no indication that any enol radical cation has been formed.[25]

3.4. Tunneling Kinetics. The observed temperature independence of the enolization of $\mathbf{DMI}^{\bullet+}$ (cf. Figure 3) and the fact that deutration of the methyl group all but shuts down this process at the temperatures attainable in Ar matrix experiments indicates very strongly that quantum mechanical tunneling is involved. We had previously been able to model the kinetics of enolizations quite successfully with the Bell model.[6] This simple model[26] assumes a barrier of parabolic shape that has—at the vibrational level at which a particle of mass m tunnels—a width b and a heigth E_a. Under these premises, the correction factor $Q(T)$ that must be applied to the classical Arrhenius rate constant $k_A(T) = A\ \exp(-E_a/RT)$ takes the simple form

$$Q(T) = \frac{e^{\alpha}}{\beta - a}(\beta \cdot e^{-\alpha} - \alpha \cdot e^{-\beta})$$

where

$$\alpha = \frac{E_a}{RT} \quad \text{and} \quad \beta = \frac{\pi^2}{h} b\sqrt{2mE_a}$$

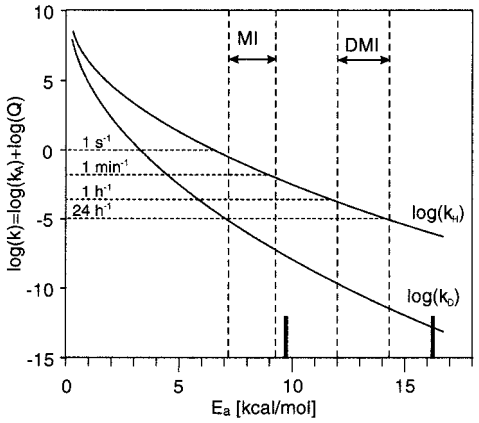

Figure 10. Plot of $\log(k) = \log(k_A) \cdot \log(Q)$ vs E_a for hydrogen or deuterium atom transfer by quantum mechanical tunneling trough a parabolic barrier of 1.25 Å width at 12 K (where the contribution of k_A is negligible for E_a > 3 kcal/mol) according to the Bell model (see text). Vertical dashed lines delineate the ranges of E_a that are compatible with experimental observations for $\mathbf{MI}^{\bullet+}$ and $\mathbf{DMI}^{\bullet+}$, respectively. The black bars at the bottom represent the barriers calculated by B3LYP/6-31G*.

This model predicts correctly that the overall rate becomes nearly independent of temperature at the cryogenic temperatures that prevail in our experiments, and that the kinetic isotope effect becomes very large for barriers of the kind that we are concerned with in the present case.[27] According to our calculations, the hydrogen atom must travel over a distance of $b \approx 1.25$ Å in the methylindanone radical cations that are at the focus of our study.[28] In Figure 10 we plot the rate constant $\log(k) = \log(k_A) + \log(Q)$ for T = 12 K and b = 1.25 Å. Thereby we used A(12 K) = 1.83×10^{10} s^{-1} which we derived from $\Delta S^{\ddagger}$ = −30 J·mol^{-1}·K^{-1} calculated by B3LYP/6-31G* for $\mathbf{MI}^{\bullet+}$ and the corresponding transition state **TS1** for its enolization.

From our experiments we know that in the case of $\mathbf{MI}^{\bullet+}$ the rate must be in the s^{-1} to min^{-1} range, whereas the lifetime of $\mathbf{MI}$-$d_3{}^{\bullet+}$ must be in the dozens of hours ($\log(k) < 10^{-5}$ s^{-1}). On the other hand, the rate of enolization of $\mathbf{DMI}^{\bullet+}$ is in the h^{-1} range ($\log(k) = 10^{-4}$−10^{-5} s^{-1}).

The above observations define ranges for E_a of the enolization in the methylindanone radical cations which are indicated by vertical dashed lines in Figure 10. It is interesting to note that the difference in E_a for enolization of $\mathbf{MI}^{\bullet+}$ and $\mathbf{DMI}^{\bullet+}$ is in same range as the difference in the classical barriers computed

(24) If we take both states at their relaxed geometries this difference amounts to 5.2 kcal/mol. However, the lowest point on the conical intersection subspace between the π- and the σ-radical states, through which the reaction must proceed if it follows a classical mechanism, will lie at a higher energy.

(25) Zhu, Z. Ph.D. Thesis No. 1152, University of Fribourg, Switzerland, 1997.

(26) Caldin, E. F. *Chem. Rev.* **1969**, *69*, 135.

(27) Bednarek, P. Ph.D. Thesis No. 1301, University of Fribourg, Switzerland, 2000.

(28) The distance b is 1.28 Å if the reaction occurs from the π-radical state, 1.22 Å if it occurs from the π-radical state. The dependence of the tunneling rates on b is not very pronounced, therefore we chose the average value for our simulations.

Table 4. Excited States of **DMI**$^{\bullet+}$.

TD-PBE0[a]		TD-B3LYP[a]		CASPT[b]		exptl[c]	main excitation CASSCF[b,f]	
ΔE [eV]	f[d,e]	ΔE [eV]	f[d,e]	ΔE [eV]	f[d]	ΔE [eV]		
0.32	$<10^{-4}$	0.09	$<10^{-4}$	0.81	1×10^{-6}		87%	$n_O \rightarrow \pi_4$
0.98	$<10^{-4}$	0.90	0.0004	0.80	0.0002		83%	$\pi_3 \rightarrow \pi_4$
2.77	0.0047	2.63	0.0350	2.69	0.0313	2.58	57%	$\pi_2 \rightarrow \pi_4$
							9%	$\pi_3 \rightarrow \pi_6$
							9%	$\pi_4 \rightarrow \pi_5$
3.50	0.0024	3.36	0.0227	3.84	0.0297	>4.1	29%	$\pi_1 \rightarrow \pi_4$
							17%	$\pi_2 \rightarrow \pi_4$
3.92	0.0021	3.91	0.0121	4.04	0.160	>4.1	27%	$\pi_4 \rightarrow \pi_5$
							15%	$\pi_3 \rightarrow \pi_6$
							13%	$\pi_1 \rightarrow \pi_4$

[a] Calculated with the 6-31G* basis set. Note that both TD-DFT methods predict additional transitions[37] that are, however, too weak to be observed or lie outside the observation range. [b] Calculated with the ANO-L basis set, active space: (15,12)/[1σ,11π]. [c] See the spectrum of **DMI-d_3**$^{\bullet+}$ in Figure 4a. [d] Oscillator strength for electronic transition. [e] The absolute values of the oscillator strengths from the TD-DFT output of Gaussian 98 cannot be compared to those from the CASPT2 calculations.[58] [f] See MOs in Figure 11.

Table 5. Excited States of **MI**$^{\bullet+}$

TD-PBE0[a]		TD-B3LYP[a]		CASPT[b]		exptl[c]	main excitation CASSCF[b,f]	
ΔE [eV]	f[d,e]	ΔE [eV]	f[d,e]	ΔE [eV]	f[d]	ΔE [eV]		
0.10	$<10^{-4}$	−0.14	$<10^{-4}$	0.42	4×10^{-8}	−	88%	$n_O \rightarrow \pi_4$
0.82	$<10^{-4}$	0.74	$<10^{-4}$	0.65	6×10^{-6}	−	81%	$\pi_3 \rightarrow \pi_4$
2.62	0.0036	2.48	0.0283	2.73	0.0328	2.58	54%	$\pi_2 \rightarrow \pi_4$
							12%	$\pi_3 \rightarrow \pi_6$
3.41	0.0016	3.29	0.0195	3.61	0.0029	>4.1	37%	$\pi_2 \rightarrow \pi_4$
							34%	$\pi_1 \rightarrow \pi_4$
4.62	0.0068	4.53	0.0392	4.30	0.1447	>4.1	71%	$\pi_4 \rightarrow \pi_5$

[a] Calculated with the 6-31G* basis set. Note that both TD-DFT methods predict additional transitions to those listed above[37] that are, however, too weak to be observed or lie outside the observation range with the 6-31G* basis set. [b] With the ANO-L basis set, active space: (15,12)/[3σ,9π]. [c] See the spectrum of **MI-d_3**$^{\bullet+}$ in Figure 5c. [d] Oscillator strength for electronic transition. [e] The absolute values of the oscillator strengths from the TD-DFT output of Gaussian 98 cannot be compared to those from the CASPT2 calculations[58] [f] See MOs in Figure 11.

by B3LYP/6-31G* (solid bars at the bottom). However, these barriers are too low in both cases, which is not surprising in view of our above coupled cluster calculations on **MA**$^{\bullet+}$ which indicate that B3LYP/6-31G* overestimates barriers for such enolizations by a few kcal/mol. If one corrects for this, then the calculated barriers fall within the ranges predicted by the Bell model. But then a more sophisticated treatment of tunneling, paired with a more reliable estimate of the thermal barrier, would probably be needed to arrive at an entirely consistent picture of the kinetics of the enolization of methylindanone radical cations.

One question that remains to be answered is why, in view of the long lifetime of **MI-d_3**$^{\bullet+}$ generated photochemically from the correspondig enol radical cation (Figure 5c), a substantial amount of this enol radical cation is present after ionizaton, in contrast to **DMI-d_3**$^{\bullet+}$, where no enolization is observed on ionization (Figure 4a). The reason for this is that on charge transfer from Ar (which is the predominant ionization mechanism of embedded substrates on X irradiation of Ar matrices[29]) the incipient substrate radical cations are imparted with a substantial amount of excess energy that they cannot easily dissipate in solid Ar. This excess energy is therefore available to drive thermal rearrangements, such as the present tautomerizations. The extent to which such reactions occur depends on the heigth of the barriers to be crossed. Apparently, this barrier is low enough in **MI**$^{\bullet+}$ but too high in **DMI**$^{\bullet+}$, in accord with the calculated 6.5 kcal/mol difference.

3.5. Electronic Structure of the Observed Radical Cations. Above we had claimed that the observed spectra of **DMI**$^{\bullet+}$ (Figure 4a) and **MI**$^{\bullet+}$ (Figure 5c) are only compatible with a π-radical ground-state structure of the two species. We wish to substantiate this claim by electronic structure calculations which will also encompass the corresponding enol radical cations, **DME**$^{\bullet+}$ and **ME**$^{\bullet+}$, observed in our experiments. To this end we carried out CASSCF/CASPT2 calculations which have proven to yield rather reliable predictions of excited-state energies and electric dipole transition moments in previous applications to radical cation spectra.[18,30−35] In addition we did some calculations with the recently introduced methods based on time-dependent density functional response theory (TD-DFT).[36]

The results of these calculations which were all carried out at the B3LYP equilibrium geometries of the radical cations are listed in Tables 4−7 and indicated graphically by gray bars in Figures 1, 4, and 5. From these data we gather that the CASPT2 predictions are generally in good agreement with experiment, in line with previous findings for similar cases.[10,18] The most conspicuous deviation is found for the third excited state of the enol radical cations (cf. Figures 1c and 5d), but even this deviation is within the expected limits of accuracy of this model (±0.2 eV). The agreement of the predictions by the much more

(29) Bally, T. In *Radical Ionic Systems*; Lund, A., Shiotani, M., Eds.; Kluwer: Dordrecht, The Netherlands, 1991.
(30) Fülscher, M. P.; Matzinger, S.; Bally, T. *Chem. Phys. Lett.* **1995**, *236*, 167.
(31) Zhu, Z.; Bally, T.; Wirz, J.; Fülscher, M. *J. Chem. Soc., Perkin Trans. 2* **1998**, 1083.
(32) Bally, T.; Carra, C.; Fülscher, M. P.; Zhu, Z. *J. Chem. Soc., Perkin Trans. 2* **1998**, 1759.
(33) Bally, T.; Carra, C.; Matzinger, S.; Truttmann, L.; Gerson, F.; Schmidlin, R.; Platz, M. S.; Admasu, A. *J. Am. Chem. Soc.* **1999**, *121*, 7011.
(34) Marcinek, A.; Adamus, J.; Huben, K.; Gebicki, J.; Bartczak, T. J.; Bednarek, P.; Bally, T. *J. Am. Chem. Soc.* **2000**, *122*, 437.
(35) Bally, T.; Bernhard, S.; Matzinger, S.; Roulin, J.-L.; Sastry, G. N.; Truttmann, L.; Zhu, Z.; Marcinek, A.; Adamus, J.; Kaminski, R.; Gebicki, J.; Williams, F.; Chen, G.-F.; Fülscher, M. R. *Chem. Eur. J.* **2000**, *6*, 858.
(36) Casida, M. E. In *Recent Advances in Density Functional Methods*, Part I; Chong, D. P., Ed.; World Scientific: Singapore, 1995; p 155.

Table 6. Excited States of **DME**$^{\bullet+}$

TD-PBE1PBE		TD-B3LYP		CASPT[b]		exptl[c]	main excitation CASSCF[b,d]	
ΔE [eV]	f	ΔE [eV]	f	ΔE [eV]	f	ΔE [eV]		
2.23	0.0020	2.16	0.0206	7×10^{-4}	1.87	1.74	52%	$\pi_4 \rightarrow \pi_5$
							−26%	$\pi_3 \rightarrow \pi_4$
2.90	0.0052	2.86	0.0431	0.0500	2.58	2.53	66%	$\pi_2 \rightarrow \pi_4$
3.15	0.0128	3.11	0.1142	0.0328	2.73	2.95	42%	$\pi_3 \rightarrow \pi_4$
							+12%	$\pi_4 \rightarrow \pi_5$
3.75	0.0026	3.71	0.0094	0.1447	4.30		37%	$\pi_4 \rightarrow \pi_6$
							−11%	$\pi_2 \rightarrow \pi_5$
							−11%	$\pi_1 \rightarrow \pi_4$

[a] With the 6-31G* basis set. [b] With the ANO-L basis set, active space: (15,12)/[1σ,11π]. [c] See the spectrum of **DME**$^{\bullet+}$ in Figure 1c. [d] See MOs in Figure 11.

Table 7. Excited States of **ME**$^{\bullet+}$

TD-PBE1PBE		TD-B3LYP		CASPT[b]		exptl[c]	main excitation CASSCF[b,d]	
ΔE [eV]	f	ΔE [eV]	f	ΔE [eV]	f	ΔE [eV]		
2.35	0.0024	2.26	0.0241	1.93	0.0024	1.88[e]	52%	$\pi_4 \rightarrow \pi_5$
							−24%	$\pi_3 \rightarrow \pi_4$
2.89	0.0034	2.84	0.0361	2.61	0.0383	2.58	63%	$\pi_2 \rightarrow \pi_4$
3.26	0.0117	3.25	0.0969	2.78	0.1213	3.00	38%	$\pi_3 \rightarrow \pi_4$
							+20%	$\pi_4 \rightarrow \pi_5$
3.82	0.0056	3.76	0.0283	3.75	0.0310	3.64	31%	$\pi_4 \rightarrow \pi_6$
							−12%	$\pi_2 \rightarrow \pi_5$
							−11%	$\pi_1 \rightarrow \pi_4$

[a] With the 6-31G* basis set. [b] With the ANO-L basis set, active space: (15,12)/[1σ,11π]. [c] See the spectra in Figure 5a,d. [d] See MOs in Figure 11. [e] Average between vertical excitation energies in the first band of **ME**$^{\bullet+}$ and **ME-d_3**$^{\bullet+}$.

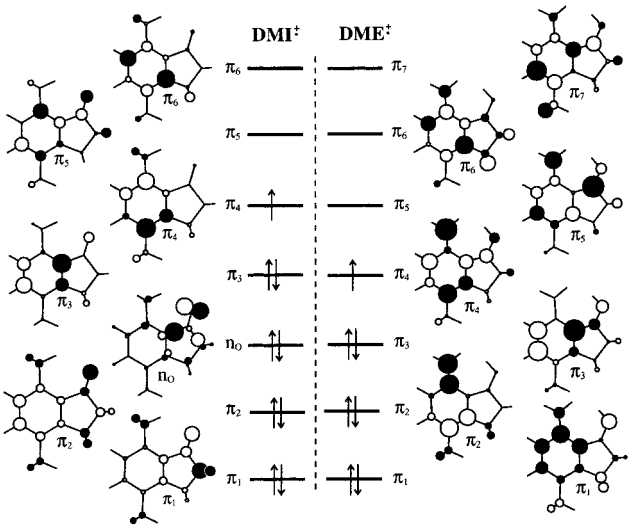

Figure 11. Moplot representation of the molecular orbitals involved in the excitations of **DMI**$^{\bullet+}$ and **DME**$^{\bullet+}$ listed in Tables 4 and 6. The corresponding orbitals for **MI**$^{\bullet+}$ and **ME**$^{\bullet+}$ (cf. Tables 5 and 7) look very similar.

economical TD-DFT methods with the observed bands is generally also satisfactory, although not as good on the average as those obtained at the CASPT2 level. However, substantial discrepancies are found between the TD-DFT and the CASPT2 predictions for the first excited state of **MI**$^{\bullet+}$ and **DMI**$^{\bullet+}$, which arises by promotion of an electron from the n_O to the π_4 MO (or by electron ejection from the n_O MO in the neutral precursors). This state is predicted much too low, especially by TD-B3LYP which even places it 3.2 kcal/mol *below* the ground state at its equilibrium geometry! This is all the more surprising as the same state was predicted to lie 8.7 kcal/mol *above* the π-radical ground state by separate B3LYP calculations on these two states, in excellent accord with CASPT2 which predicted this gap to be 9.7 kcal/mol (see Table 1). The same discrepancy between B3LYP and its TD variant is found for **DMI**$^{\bullet+}$ (14.0 vs 2.0 kcal/mol, respectively). Since the two electronic states in question are described well by single configurations this divergent behavior of the two flavors of DFT theory is puzzling. Apparently TD-DFT is poorly suited to describe relative energies of π-radical and σ-radical states in radical ions, and perhaps also in neutral compounds (n $\rightarrow \pi^*$ vs $\pi \rightarrow \pi^*$ excitations).

Apart from the above low-energy $n_O \rightarrow \pi_4$ and $\pi_3 \rightarrow \pi_4$ excitations, the electronic structure of the methylindanone radical cations is unsurprising.[37] As is often found in radical cations, the lowest few excited states are described by electron promotions from doubly occupied MOs to the singly occupied MO (SOMO). Excitations into virtual orbitals only come into play in the UV range (see Tables 4 and 5). In contrast, the quinoid chromophore of the enol radical cations gives rise to a pair of excited states arising from linear combination of the SOMO-1 $\rightarrow$ SOMO ($\pi_3 \rightarrow \pi_4$) and SOMO $\rightarrow$ LUMO excitations, as is typical for polyenic radical cations.[30] These excitations lead to a weak red (negative linear combination) and a strong blue absorption (positive linear combination) in the spectrum. Between the two lies the second excited state formed by $\pi_2 \rightarrow \pi_4$ excitation. According to CASPT2 the sharp peak at ca. 340 nm in **MI**$^{\bullet+}$ (Figure 5) is due to $\pi_2 \rightarrow \pi_6$ excitation (cf. MOs on the right side of Figure 11).

Finally, we calculated also the electronic spectrum that would be expected if **MI**$^{\bullet+}$ had a σ-radical ground state, a possibility that we had to admit in view of the results shown in Figure 9. However, according to TD-B3LYP only a very weak transition is expected in the range of the intense absorption of ionized **MI**, whereas a rather strong one is predicted to occur around 340 nm where the observed spectrum shows no bands. In addition, the IR spectrum of **MI-d_3**$^{\bullet+}$ (not shown) shows a strong

(37) In addition to the transitions that are listed in Tables 4 and 5, the TD-DFT methods predict a number of $n_O \rightarrow \pi^*$ transitions that carry, however, very small oscillator strengths. Hence they do not manifest themselves in the experimental spectra and they were therefore not calculated by CASPT2 and are not listed in the tables. Also, TD-DFT predicts more $\pi \rightarrow \pi^*$ transitions than CASPT2 in the UV region but these are also not listed because they lie outside the present observation range. The full results of the TD-DFT calculations are available in the Supporting Information..

band at 1749 cm^{-1}, in accord with the B3LYP prediction for the $^2A''$ state (1785 cm^{-1} after scaling by 0.97), but in stark disagreement with the prediction for the $^2A'$ state where the C═O stretching mode is shifted to 1478 cm^{-1} (after scaling by 0.97). Thus we conclude that **MI** ends up predominantly in the π-radical minimum on ionization, although vertical electron loss favors the σ-radical state according to B3LYP (and, marginally, also to CASPT2).

4. Conclusions

The radical cation formed on ionization of 4,7-dimethylindanone in Ar at 12 K is stable for hours but undergoes slow tautomerization at a rate that is independent of temperature up to 30 K. The resulting enol radical cation can be reverted photochemically to the keto form. In contrast, the 7-methylindanone radical cation does not persist under these conditions but decays spontaneously to the corresponding enol radical cation which furthermore appears to be photostable. Deuteration of the methyl groups completely suppresses enolization in both methylindanone radical cations, such that ionized 7-methylindanone can now be observed leisurly, too.

The surprising effect of the 4-methyl group, which is distant from the site of tautomerization, can be traced back to an electronic factor, i.e., the stabilization of the unreactive π-radical relative to the reactive σ-radical state of the methylindanone radical cation. B3LYP calculations of the reaction profile show that the difference in activation energies can be largely accounted for by the promotion from the π-radical to the σ-radical state that is nearly thermoneutral in the 7-methylindanone but requires about 6.5 kcal/mol in the 4,7-dimethylindanone case. This example represents the first demonstration of state selectivity in radical ion rearrangements. The above observations and simulations of the observed kinetics on the basis of the Bell model for hydrogen atom tunneling show that this is the dominant mechanism for enolization, in agreement with previous findings on related systems.[8,9]

It has been known for a while that aromatic ketones whose lowest lying triplet states are of $\pi \rightarrow \pi^*$ nature are notoriously less reactive in photoreduction (H-abstraction) than those where they are of $n \rightarrow \pi^*$ nature.[38,39] The cause of this difference in reactivity is the same as that which appears to be operative in the present case, i.e., the presence or absence of a singly occupied n_O orbital in one or the other electronic state of the ketone (or its radical cation). However, the exact mechanism by which this difference in reactivity, which increases smoothly as the energy difference between the two states changes, comes about is still a matter of debate (thermal equilibration or vibronic coupling between with the two states).[12,40]

To our best knowledge, the question of state selectivity has never been addressed in photoenolizations involving *o*-alkyl aromatic ketones, which are, however, known to have close-lying $n \rightarrow \pi^*$ and $\pi \rightarrow \pi^*$ triplet states.[41] It would come as no surprise if substituents wold have an equally dramatic effect on the rate of enolization as has been found in the present case of radical cations.

5. Experimental Section

5.1. Syntheses: (a) 4,7-Dimethylindanone (DMI) was made by $H_2SO_4/AlCl_3$ catalyzed cyclization of 2′,5′-dimethyl-3-chloropropiophenone according to one of the procedures described by Khalaf et al.[42] A solution of β-chloropropionyl chloride (0.105 mol) and *p*-xylene (0.1 mol) in 13 mL of CS_2 was added slowly to a mixture of 16 g of $AlCl_3$ and 65 mL of CS_2. After the mixture was stirred for 3 h at room temperature, the CS_2 was removed under vacuum and 125 mL of concentrated H_2SO_4 was added to the remaining oily residue. The mixture was heated to 90 °C for 45 min, then cooled and poured onto ice. The resulting solid was extracted with diethyl ether and benzene. The extracts were washed with sodium carbonate solution and water and dried over sodium sulfate, and the solvents were removed under vacuum. The crude product was crystallized from methanol (68%, mp 77 °C, lit.[42] mp 76−77 °C).

(b) 4,7-Bis(trideuteriomethyl)indanone (DMI-d_6)[13] was prepared analogous to DMI starting from perdeuterated *p*-xylene.

(c) 7-Methylindanone was made by cyclization of 3-methylhydrocinnamic acid with polyphosphoric acid, a procedure that has been employed successfully for the synthesis of a range of substituted indanones.[43] Typically, a mixture of 1 g of 3-methylhydrocinnamic acid in 7 mL of polyphosphoric acid was heated to 80 °C for 3 h with occasional stirring. The reaction mixture was poured into water and extracted with diethyl ether. The mixture of 5-methyl- and 7-methylindanone that was obtained in this way was separated by column chromatography on silica 60F with methylene chloride to give **MI** in about 38% yield (mp 52−54 °C, lit.[44] mp 54.7−55.2 °C; ^1H NMR, IR, and UV spectra in accord with literature reports[44,45]).

(d) 3-Methylhydrocinnamic acid was obtained by Perkin condensation[46] of 3-methylbenzaldehyde with acetic anydride in the presence of potassium acetate and subsequent reduction of the cinnamic acid with sodium amalgam.[47] 3-Methylbenzaldehyde (5 mL, 7.7 g; Fluka) and 4 g of AcOK were dissovled in 9 mL of Ac_2O and heated to 155 °C in a dry flask for 6 h. The resulting reaction mixture was poured onto 100 mL of water and alkalified with sodium carbonate. Diethyl ether extracts were washed with water and dilute HCl whereupon the crude cinnamic acid was filtered and recrystallized from EtOH (yield 6.5 g, 84%, mp 114 °C). For the reduction, a solution of 1 g of 3-methylcinnamic acid in 15 mL of 1 M NaOH was added during 15 min to 16 g of sodium amalgam and kept at 50 °C for two more hours after the addition was terminated. After decanting the mercury the product was washed with water and the aqueous phases were acidified with 50% HCl. The crude product was then exctracted with diethyl ether. After drying and evaporation, 740 mg of a clear pale yellow oil was obtained which spontaneously crystallized on standing (mp 38−42 °C, lit.[47] mp 42−43 °C).

(e) 7-(Trideuteriomethyl)indanone (MI-d_3) was prepared analogous to **MI** starting from 3-(trideuteriomethyl)benzaldehyde that was obtained by reductive condensation of 3-bromobenzaldehyde with CD_3I following the procedure described by Chapman et al.[48] To avoid deuterium exchange in the methyl group during the cinnamic acid reduction, we substituted NaOH by NaOD, which led of course to incorporation of two deuterium atoms in the propionic acid chain. However, during the subsequent cyclization with polyphosphoric acid, these deuterium atoms were partially lost again. Mass spectra indicated that the final product still contained one additional deuterium atom that according to the ^1H NMR spectrum is located β to the carbonyl group. However, as the presence of this additional deuterium atom was not expected to change the spectroscopic properties of interest in the present study, no efforts were made to arrive at a sample of isotopically pure **MI-d_3** (which, strictly speaking, we should therefore call **MI-d_4**).

5.2. Matrix Isolation and Spectroscopy. Crystals of the compounds were placed in a U-shaped tube immersed into a water bath and connected to the inlet system of a closed-cycle cryostat. While the bath

(38) Pitts, J. N.; Johnson, H. W.; Kuwana, T. *J. Phys. Chem.* **1962**, *66*, 2456.
(39) Wagner, P. J.; Kemppainen, A. E. *J. Am. Chem. Soc.* **1968**, *90*, 5898.
(40) Wagner, P. J. In *Rearrangements in Ground and Excited States*; de Mayo, P., Ed.; Academic Press: New York, 1980; Vol. 3, p 381.
(41) Lamola, A. A. *J. Chem. Phys.* **1967**, *47*, 4810.
(42) Khalaf, A. A.; Abdel-Nahab, A. M. A.; El-Khawaga, A. M.; El-Zahry, M. F. *Bull Soc. Chim. Fr. Part II* **1984**, 285.
(43) Koo, J. *J. Am. Chem. Soc.* **1953**, *75*, 1891.
(44) House, H. O.; Rasmusson, G. H. *J. Org. Chem.* **1963**, *28*, 31.
(45) Buys, T. S. V.; Cerfontain, H.; Geenevasen, J. A. J.; Stunnenberg, F. *Recl. Trav. Chim. Pays-Bas* **1986**, *105*, 188.
(46) Johnson, J. R. In *Organic Reactions*; Wiley & Sons: New York, 1942; Vol. 1, p 210.
(47) Dippy, J. F. J.; Page, J. E. *J. Chem. Soc.* **1938**, *1938*, 357.
(48) Chapman, O. L.; Johnson, J. W.; McMahon, R. J.; West, P. R. *J. Am. Chem. Soc.* **1978**, *110*, 508.

was kept between 0 and −10 °C (depending on the total surface of the crystals in the U-tube) a mixture of argon and CH_2Cl_2 (1000:1) was flowing through the tube at a rate of ≈1 mmol/h and swept the compounds onto a CsI window held at 19 K. There the mixture accumulated to form a matrix containing a sufficient quantity of the compound within 2 h.

After taking reference spectra, the samples were exposed to 90 min of X-irradiation as described previously.[29] Photolyses were effected with a 1 kW Ar plasma discharge lamp through appropriate low-pass cutoff or interference filters. Electronic absorption (EA) spectra were taken between 200 and 1200 nm with a Perkin-Elmer Lambda 19 instrument, whereas IR spectra were obtained on a Bomem DA3 interferometer (1 cm^{-1} resolution) equipped with an MCT detector (500−4000 cm^{-1}).

Gas-phase photoelectron spectra were measured on a modified Perkin-Elmer PE 16 instrument operated in pre-retardation (and hence constant resolution) mode.[49] Calibration was effected with a Xe−Ar mixtured and the spectral resolution was about 20 meV.

5.3. Quantum Chemical Calculations. The geometries of all species were optimized by the B3LYP density functional method[50,51] as implemented in the Gaussian 98 programs,[52,53] using the 6-31G* basis set. Relative energies and vibrational spectra were calculated at the same level. Full sets of Cartesian coordinates and absolute energies (including thermal corrections where available) are given in the Supporting Information.

Excited-state calculations were carried out at the B3LYP/6-31G* geometries of the radical cations (except where indicated otherwise) by the CASSCF/CASPT2 procedure[54] with the MOLCAS program[55] using the [C,N,O]3s2p1d/[H]2s ANO basis set.[56] The active spaces were chosen such as to obtain a satisfactory description of all excited states of interest at the CASPT2 level. The resulting active spaces are described in the footnotes to Tables 4−7. To ensure orthogonality, the CASSCF wave functions were averaged over all excited states of the same symmetry. Transition moments were calculated on the basis of these wave functions, using CASPT2 energy differences in the denominator.

In addition we resorted to a recently introduced molecular density functional method based on time-dependent response (TDR) theory,[36] according to which the poles and the residues of the frequency-dependent polarizability are evaluated, where the former correspond to vertical excitation energies and the latter to oscillator strengths. Analogous to the Hartree−Fock variant of TDR (in the popular Tamm−Dancoff or Random−Phase approximation), excited states are then described in terms of CI vectors containing single excitations from a ground state wave function (CIS), which makes for a very transparent interpretation of the results. However, it should be noted that the treatment of electron correlation in TD density functional response theory (TD-DFT) goes far beyond that in a HF-based CIS method which makes the results generally more accurate.

We used the variant of TD-DFT described recently by Stratmann et al.[57] and implemented in the Gaussian 98 program.[52,58] Next to the B3LYP functional we employed also a recently introduced hybrid variant of the nonempirical Perdew−Burke−Ernzerhof (PBE) functional[59−61] that was shown to be well suited for the evaluation of excitation energies of radicals.[62] The results obtained with the two functionals differ somewhat, but one is not consistently in better agreement with experiment than the other.

The MOs in Figures 6 and 11 were plotted with the Moplot program,[63] which gives a schematic representation of the MO's nodal structure within a ZDO-type approximation.[64]

Acknowledgment. This paper is dedicated to Prof. Edwin Haselbach (University of Fribourg) on occasion of his 60th birthday, in gratitude for his continuing advice, for many exciting discussions, and for his friendship. This work was supported by the Swiss National Science Foundation (Project No. 2000-061560.00) and by grants from the Polish State Committee for Scientific Research (No. 3/T09A/122/18). We are very indebted to Prof. Michael Allan and Anne-Christelle Sergenton (University of Fribourg) for measuring the photoelectron spectra shown in Figure 6.

Supporting Information Available: Energies and Cartesian coordinates from the B3LYP calculations for all stationary points mentioned in this study (minima and transition states) as well as full results from TD-B3LYP calculations (ASCII). This material is available free of charge via the Internet at http://pubs.acs.org.

JA003708M

(49) Dressler, R.; Neuhaus, L.; Allan, M. *J. Electron Spectrosc. Relat. Phenom.* **1983**, *31*, 181.

(50) Becke, A. D. *J. Chem. Phys.* **1993**, *98*, 5648.

(51) Lee, C.; Yang, W.; Parr, R. G. *Phys. Rev. B* **1988**, *37*, 785.

(52) Frisch, M. J.; Trucks, G. W.; Schlegel, H. B.; Scuseria, G. E.; Robb, M. A.; Cheeseman, J. R.; Zakrzewski, V. G.; Montgomery, J. A.; Stratmann, R. E.; Burant, J. C.; Dapprich, S.; Millam, J. M.; Daniels, A. D.; Kudin, K. N.; Strain, M. C.; Farkas, O.; Tomasi, J.; Barone, V.; Cossi, M.; Cammi, R.; Mennucci, B.; Pommelli, C.; Adamo, C.; Clifford, S.; Ochterski, J.; Petersson, G. A.; Ayala, P. Y.; Cui, Q.; Morokuma, K.; Malick, D. K.; Rabuck, A. D.; Raghavachari, K.; Foresman, J. B.; Cioslowski, J.; Ortiz, J. V.; Stefanov, B. B.; Liu, G.; Liashenko, A.; Piskorz, P.; Komaromi, I.; Gomperts, R.; Martin, R. L.; Fox, D. J.; Keith, T.; Al-Laham, M. A.; Peng, C. Y.; Nanayakkara, A.; Challacombe, M.; Gill, P. M. W.; Johnson, B. G.; Chen, W.; Wong, M. W.; Andres, J. L.; Gonzales, C.; Head-Gordon, M.; Repogle, E. S.; Pople, J. A. Gaussian 98; Rev. A1 ed.; Gaussian, Inc.: Pittsburgh, PA, 1998.

(53) Johnson, B. G.; Gill, P. M. W.; Pople, J. A. *J. Chem. Phys.* **1993**, *98*, 5612.

(54) Andersson, K.; Roos, B. O. In *Modern Electronic Structure Theory*; World Scientific Publ. Co.: Singapore, 1995; Part 1, Vol. 2, p 55.

(55) Andersson, K.; Blomberg, M. R. A.; Fülscher, M. P.; Kellö, V.; Lindh, R.; Malmqvist, P.-Å.; Noga, J.; Olson, J.; Roos, B. O.; Sadlej, A.; Siegbahn, P. E. M.; Urban, M.; Widmark, P.-O. MOLCAS; Version 4; University of Lund: Lund, Sweden, 1998.

(56) Pierloot, K.; Dumez, B.; Widmark, P.-O.; Roos, B. O. *Theor. Chim. Acta* **1995**, *90*, 87.

(57) Stratmann, R. E.; Scuseria, G. E.; Frisch, M. J. *J. Chem. Phys.* **1998**, *109*, 8218.

(58) The transition moments that appear in the TD-DFT output of Gaussian should probably be taken with a grain of salt, because their absolute values vary by orders of magnitude depending on the number of excited states (NStates=nn) that are calculated.

(59) Ernzerhof, M.; Scuseria, G. E. *J. Chem. Phys.* **1999**, *110*, 5029.

(60) Adamo, C.; Barone, V. *J. Chem. Phys.* **1999**, *110*, 6158.

(61) The same functional was introduced simultaneously under two different names (PBE1PB[59] and PBE0[60]). It is invoked by the PBE1PBE keyword in Gaussian 98, but we list the results under the simpler heading of PBE0 in Tables 4−7.

(62) Adamo, C.; Barone, V. *Chem. Phys. Lett.* **1999**, *314*, 152.

(63) Bally, T.; Albrecht, B.; Matzinger, S.; Sastry, M. G. MOPLOT, a program for displaying results of LCAO-MO calculations, available on request from Thomas.Bally@unifr.ch.; Version 3.2 University of Fribourg, 1997.

(64) Haselbach, E.; Schmelzer, A. *Helv. Chim. Acta* **1979**, *54*, 1299.